Jour. Fac. Sci., Hokkaido Univ., Ser. IV,
vol. 17, no. 3, Feb., 1977, pp. 487-504.

THE SYSTEM $NaFe^{3+}Si_2O_6$-$CaFe^{2+}Si_2O_6$ AT LOW OXYGEN FUGACITY

by

Kohei Ohta*, Kosuke Onuma and Kenzo Yagi

(with 1 table and 8 text-figures)

(Contribution from the Department of Geology and Mineralogy,
Faculty of Science, Hokkaido University, No. 1482)

Abstract

The $CaFe^{2+}Si_2O_6$-rich part of the system $NaFe^{3+}Si_2O_6$-$CaFe^{2+}Si_2O_6$ was determined at the temperature range of 1100°C-1250°C and at oxygen fugacities of 10^{-9}, 10^{-10}, and 10^{-11} atm. It was found that a high temperature form of hedenbergite has not β-wollastonite structure, but bustamite structure in the temperature range of 1100°C-1175°C. Three Fe^{2+}-bearing silicate phases were also confirmed by X-ray diffraction patterns and optical properties: Fe-bustamite$_{ss}$, β-Fe-wollastonite$_{ss}$, and α-Fe-wollastonite$_{ss}$ (ss: solid solution). These three phases are solid solutions between $CaSiO_3$ and $FeSiO_3$ at low oxygen fugacity; $NaFe^{3+}Si_2O_6$ enters into the liquid when the crystalline phases coexist with liquid. The following phase assemblages were encountered with increasing temperature: Fe-bustamite$_{ss}$ + iron oxide + liquid, β-Fe-wollastonite$_{ss}$ + Fe-bustamite$_{ss}$ + iron oxide + liquid, β-Fe-wollastonite$_{ss}$ + iron oxide + liquid, β-Fe-wollastonite$_{ss}$ + α-Fe-wollastonite$_{ss}$ + iron oxide + liquid, and α-Fe-wollastonite$_{ss}$ + iron oxide + liquid. The assemblages are essentially the same throughout the range of oxygen fugacity investigated, except that magnetite converts to wüstite at low oxygen fugacity. Application of the system to the natural pyroxene is also given.

Introduction

From experimental study of the system acmite-diopside and the natural pyroxene from alkalic rocks, Yagi (1966) suggested that there are continuous solid solutions in the system acmite-diopside-hedenbergite. Later Ohashi (1967) confirmed the presence of a ccomplete series of solid solutions in the system acmite-hedenbergite at subsolidus temperature, and Nolan (1969) showed that continuous solid solutions exist in the subsolidus region of the system diopside-hedenbergite-acmite. However, investigations of the high temperature region in the system acmite-hedenbergite has not yet been accomplished.

Bowen et al. (1933), investigating the system CaO-FeO-SiO_2, demonstrated that β-wollastonite forms a solid solution with ferrosilite, which enters into β-wollastonite up to 70 mole percent at high temperature with the substitution

* Present Address: Nippon Cement Co., Tokyo

of Fe^{2+} for Ca. Recently, many studies on the system CaO-FeO-SiO_2 were carried out and the problems related to the structure of high temperature forms of hedenbergite are presented (Peacor and Prewitt, 1963; Prewitt and Peacor, 1964; Rutstein, 1971; Rutstein and White, 1971; Matsueda, 1973).

From his experimental study Rutstein (1971) claimed that Fe^{2+} cannot substitute for Ca more than about 10 atomic percent in the β-wollastonite structure, and that specimens containing more than 10 percent Fe^{2+} have bustamite structure. Matsueda (1973), from his study of natural specimens as well as experimental work on the system β-wollastonite-ferrosilite, concluded that the structure of iron wollastonite is different from that of β-wollastonite.

In the present study the phase diagram of the system acmite-hedenbergite is determined at the temperature range of 1100°C – 1250°C and at the oxygen fugacity (f_{O_2}) of 10^{-9} – 10^{-11} atm and the structural problem of $CaFe^{2+}Si_2O_6$ is also discussed.

Experimental Methods

The ordinary quenching method was employed for the investigation of the phase diagram.

Homogeneous glasses were prepared by melting pure chemicals in a $Pt_{90}Rh_{10}$ crucible previously saturated with iron. Pure quartz, Fe_2O_3, $CaCO_3$ and pure $Na_2Si_2O_5$ were used as sources. These homogeneous glasses were used as starting materials for quenching experiments. Starting materials were held in $Pt_{60}Rh_{40}$ envelopes in order to minimize the loss of iron and suspended in a vertical quenching furnace. A Pt-$Pt_{87}Rh_{13}$ thermocouple used to measure the temperature was calibrated at the standard melting points of Au (1062.6°C) and diopside (1391.5°C).

The atmosphere in the furnace was controlled by running mixtures of CO_2 and H_2 gas at definite ratios. Calibration for oxygen fugacity was made by examining the stability field of hematite, magnetite, and wüstite.

X-ray diffraction patterns of the crystalline phases were obtained with CuK_α radiation at 35 KV and 20 mA at room temperature. Reflections of (210) and (102) of β-wollastonite, and (204) and (204) of bustamite were obtained at a scanning speed of 1/4 degree per minute, with silicon as an external standard.

Experimental Results and Discussions

Crystalline phases

In the present experiment three different silicate phases were recognized.

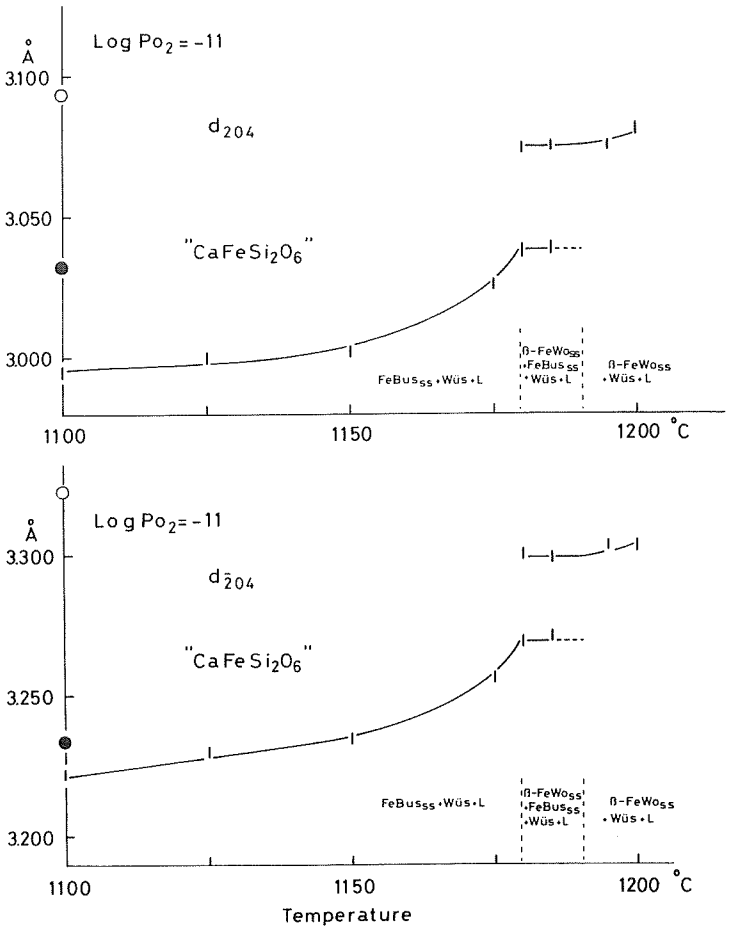

Fig. 1 Changes of d-spacings of β-Fe-wollastonite$_{ss}$ and Fe-bustamite$_{ss}$ crystallized from the composition of $CaFe^{2+}Si_2O_6$ at 10^{-11} atm f_{O_2}. The open circles represent d_{210} and d_{102} of β-wollastonite and the solid circles d_{204} and $d_{\bar{2}04}$ of bustamite. The following abbrevations will be used throughout all figures and tables. Fe-Bus = Fe-bustamite, β-Fe-Wo = β-Fe-wollastonite, α-Fe-Wo = α-Fe-wollastonite, Wüs = wüstite, Mt = magnetite.

From the X-ray diffraction patterns and optical data, it is suggested that these three crystalline phases correspond to bustamine$_{ss}$, β-wollastonite$_{ss}$, and α-wollastonite$_{ss}$. As all of these phases incorporate Fe^{2+}, henceforth these phases will be described as Fe-bustamite$_{ss}$, β-Fe-wollastonite$_{ss}$, and α-Fe-wollastonite$_{ss}$, respectively. The β-wollastonite$_{ss}$ and the α-wollastonite$_{ss}$ represent wollastonite$_{ss}$ and pseudowollastonite$_{ss}$, respectively, as defined by Bowen et al. (1933).

X-ray diffraction patterns of bustamite and β-wollastonite are similar, but

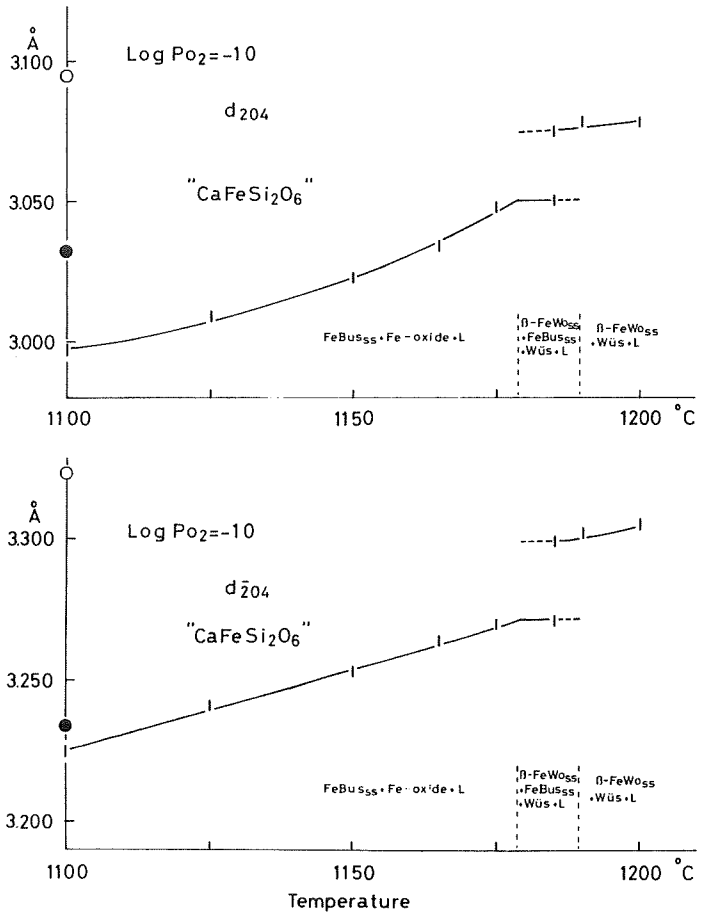

Fig. 2 Change of d-spacings of β-Fe-wollastonite$_{SS}$ and Fe-bustamite$_{SS}$ crystallized from the composition of $CaFe^{2+}Si_2O_6$ at 10^{-10} atm f_{O_2}. The open circles represent d_{210} and d_{102} of β-wollastonite and the solid circles d_{204} and $d_{\bar{2}04}$ of bustamite. Abbrevations are same as in Fig. 1.

the peaks of bustamite are located at 1-1.5° higher angle side in 2θ compared to β-wollastonite. The diffraction peaks, however, shift to the bustamite side due to Fe^{2+} substitution for Ca in the β-wollastonite structure and it may become difficult to determine whether the structure of the phases present belongs to β-wollastonite or to bustamite when β-wollastonite$_{SS}$ contains considerable amounts of Fe^{2+}.

The crystalline material of composition $CaFe^{2+}Si_2O_6$ was prepared at f_{O_2} of 10^{-11} and 10^{-10} atm to examine whether these two phases are mutually distinguishable or not. Figs. 1 and 2 show the changes of d-spacings of (204) as a function of temperature. Only one peak corresponding to that of bustamite

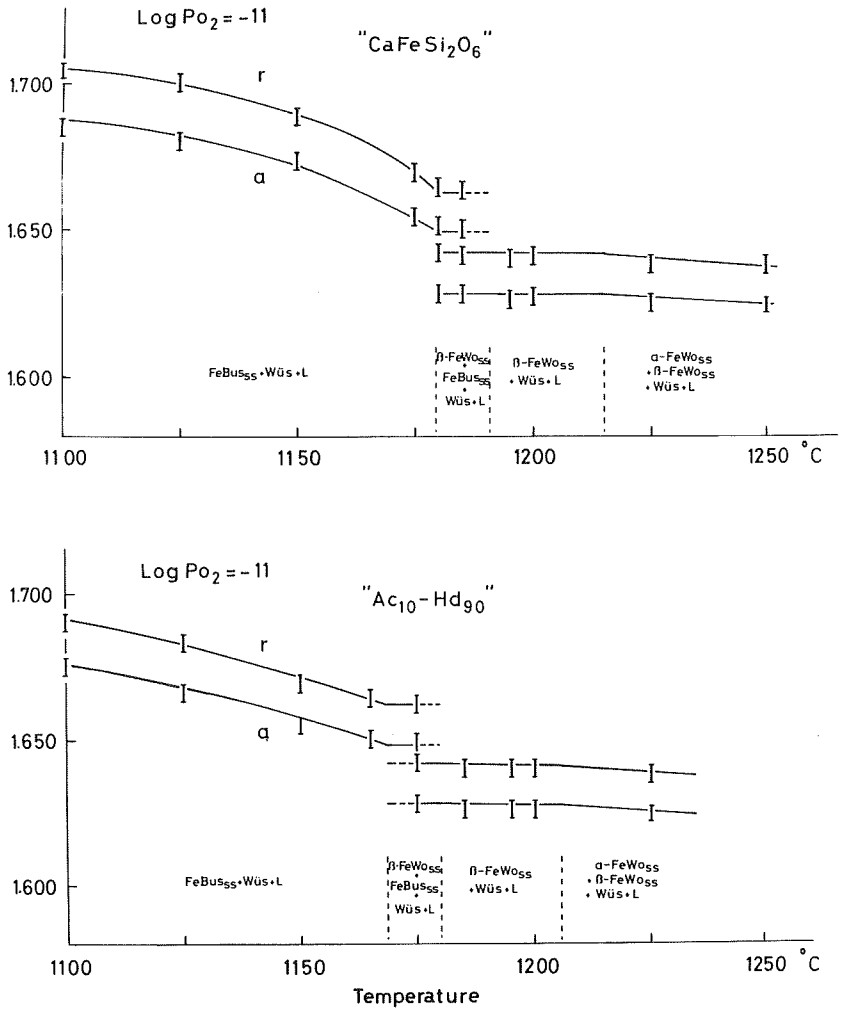

Fig. 3 Change of refractive indices of β-Fe-wollastonite$_{SS}$ and Fe-bustamite$_{SS}$ crystallized from the compositions of $CaFe^{2+}Si_2O_6$ and $Ac_{10}Hd_{90}$ at 10^{-11} atm f_{O_2}. Abbrevations are same as in Fig. 1.

was observed and the d-spacing increases with increasing temperature between 1100°C and 1175°C. The peak of (204) splits at 1180 and 1185°C, giving two different d-spacings. One is similar to the d-spacing of β-wollastonite and the other to that of bustamite. However, at higher temperatures again only one peak was observed, which gave a d-spacing similar to that of β-wollastonite (Figs. 1 and 2).

Optical methods are also useful to identify the silicate phases encountered. Two silicate phases A and B were observed in the run charges of the

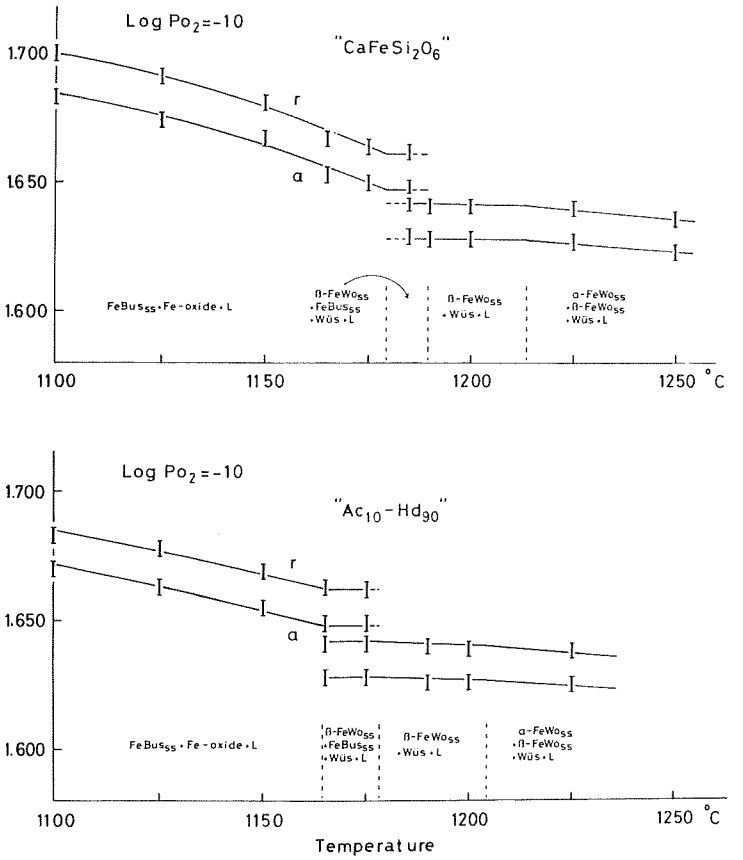

Fig. 4 Change of refractive indices of β-Fe-wollastonite$_{SS}$ and Fe-bustamite$_{SS}$ crystallized from the compositions of $CaFe^{2+}Si_2O_6$ and $Ac_{10}Hd_{90}$ at 10^{-10} atm f_{O_2}. Abbrevations are same as in Fig. 1.

composition of $CaFe^{2+}Si_2O_6$ at 1180°C and 1185°C and also that of $Ac_{10}Hd_{90}$ at 1175°C. These two phases show different refractive indices as follows: A-phase $\alpha = 1.628 \pm 0.003$, $\gamma = 1.642 \pm 0.003$; B-phase $\alpha = 1.647 \pm 0.003$, $\gamma = 1.662 \pm 0.003$. The A-phase was not encountered below these temperatures and the B-phase disappears above these temperatures. Comparing with the X-ray data it is evident that the A-phase corresponds to the β-wollastonite structure and the B-phase to the bustamite structure. The changes of refractive indices as a function of temperature are given in Figs. 3, 4, and 5. If the β-wollastonite$_{SS}$ changes in composition while maintaing its structure, the d-spacing and the refractive indices should change continuously. However, as seen in Figs. 1, 2, 3, 4, and 5, the changes of these values are discontinuous, indicating that there should be some change in the structural state. The observations mentioned above lead to the following conclusion: the phase with

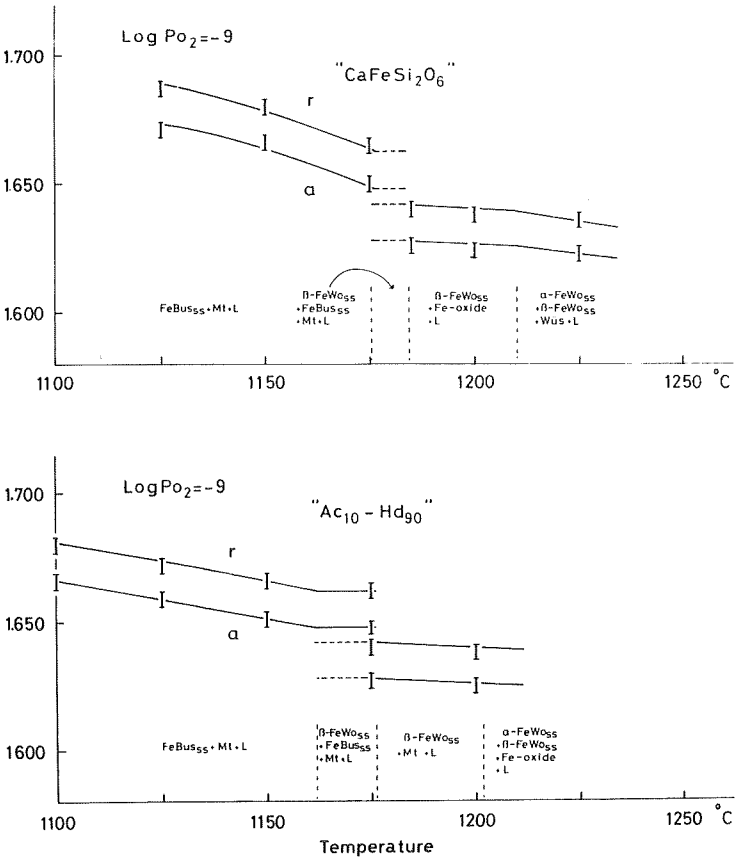

Fig. 5 Change of refractive indices of α-Fe-wollastonite$_{SS}$ and Fe-bustamite$_{SS}$ crystallized from the compositions of $CaFe^{2+}Si_2O_6$ and $Ac_{10}Hd_{90}$ at 10^{-9} atm f_{O_2}. Abbrevations are same as in Fig. 1.

low refractive indices and larger d-spacing has β-wollastonite structure, whereas the phase with high refractive indices and smaller d-spacing is presumed to have bustamite structure.

Rutstein (1971) found that bustamite with composition between $(Ca_{0.9}Fe_{0.1})SiO_3$ and $(Ca_{0.8}Fe_{0.2})SiO_3$ shows a split in the peaks of X-ray diffraction patterns, indicating the presence of two phases. He also distingushed these two phases by infrared spectral analyses and concluded that these two phases correspond to the structures of β-wollastonite and bustamite, although their optical properties were not given. Matsueda (1973) found the natural mineral to have different structure from β-wollastonite and called the structure of this mineral "iron wollastonite structure" which corresponds to the bustamite investigated by Rutstein. Since in the present study the presence of

β-wollastonite structure including Fe^{2+} is recognized in addition to α-wollastonite and bustamite structures, it is not proper to use the term "iron wollastonite" for the mineral which has a bustamite structure.

In the present investigation, therefore, the three phases mentioned above are called α-Fe-wollastonite$_{ss}$, β-Fe-wollastonite$_{ss}$ and Fe-bustamite$_{ss}$, because X-ray diffraction patterns are shifted from the pure compounds, indicating that Fe^{2+} is incorporated in the structures. Since there is some confusion concerning the structural states of these phases according to different workers, the nomenclature is compared in Table 1.

Table 1 The structural states of α-Fe-wollastonite, β-Fe-wollastonite, and Fe-bustamite by different workers.

Phase present in this study	Structural states	
	Rutstein (1971)	Matsueda (1973)
α-Fe-wollastonite	–	–
β-Fe-wollastonite	β-wollastonite	β-wollastonite
Fe-bustamite	bustamite	iron wollastonite

Under the microscope the Fe-bustamite$_{ss}$ forms nearly equant plates at lower temperatures and slender plates or prisms at higher temperatures, both being about 0.04 – 0.01 mm in length. The β-Fe-wollastonite$_{ss}$ forms slender plates or prisms, about 0.04 – 0.01 mm in length. Both of them are pale green and non-pleochroic. The α-Fe-wollastonite$_{ss}$ forms equant plates or squares, about 0.02 – 0.04 mm in size. Pleochorism is distinct as follows: X' = colorless, Z' = pale green. The α-wollastonite$_{ss}$ is distinguished from the other phases by its high birefringence. In addition to the silicate phases very small amounts of oxide minerals, magnetite and wüstite, are present throughout all runs.

Phase diagrams

Results of quenching experiments for the oxygen fugacities 10^{-11}, 10^{-10} 10^{-9} atm are listed in appendices 1, 2, and 3 with refractive indices of the silicate minerals, and the phase diagrams for each of the isobaric sections are shown in Figs. 6, 7, and 8. The transition boundary of wüstite and magnetite is calculated from the data of Darken and Gurry (1945) to locate it at 1143°C at 10^{-10} atm and 1270°C at 10^{-9} atm.

At 10^{-11} atm f_{O_2}, the following assemblages were encountered with falling temperature: α-Fe-wollastonite$_{ss}$ + wüstite + liquid, α-Fe-wollastonite$_{ss}$ + β-Fe-wollastonite$_{ss}$ + wüstite + liquid, β-Fe-wollastonite + wüstite + liquid, β-Fe-wollastonite$_{ss}$ + Fe-bustamite$_{ss}$ + wüstite + liquid, and Fe-bustamite$_{ss}$ +

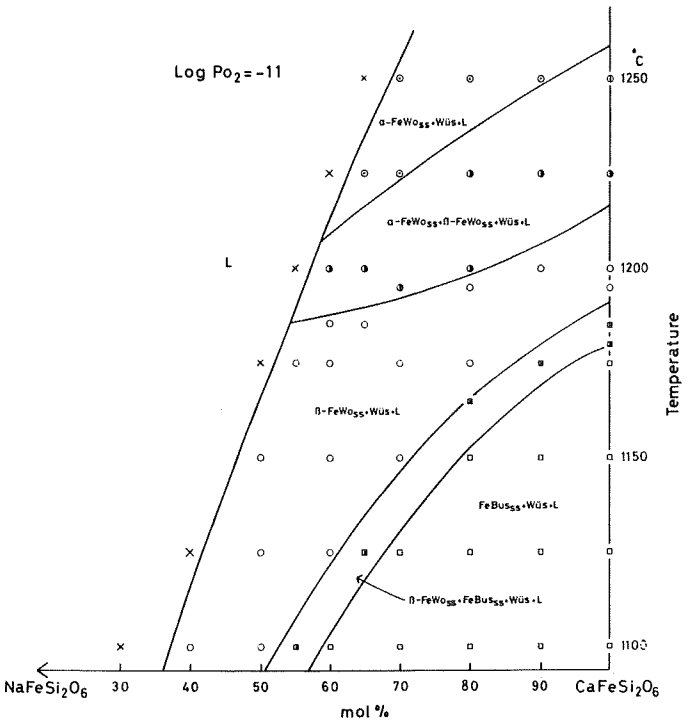

Fig. 6 Phase diagram of the system $NaFe^{3+}Si_2O_6$-$CaFe^{2+}Si_2O_6$ at 10^{-11} atm f_{O_2}. Abbrevations are given in Fig. 1.

wüstite + liquid. In the sections with f_{O_2} of 10^{-10} and 10^{-9}, the same assemblages were confirmed, except that wüstite converts to magnetite at lower temperatures.

In each section it is observed that the upper stability of each phase assemblage increases with increasing $CaFe^{2+}Si_2O_6$ and also that the stability field of each assemblage increases with decreasing f_{O_2}. On the other hand, the liquid field extends towards $CaFe^{2+}Si_2O_6$ with increasing f_{O_2}.

Since the present system is a join of a five-component system, Na_2O-CaO-Fe-O-SiO_2, the iso-fugacity T-X section is not binary, but pseudo-binary. When the composition is projected from the oxygen apex onto the Fe-SiO_2 line, magnetite and wüstite are compositionally coincident, so that the system is treated as a four-component system in the analysis of phase assemblages (see Lindsley et al., 1968). Therefore, a five-phase assemblage is univariant and a four-phase assemblage is divariant. In the 10^{-11} atm section two divariant assemblages are present, β-Fe-wollastonite$_{ss}$ + Fe-bustamite$_{ss}$ + wüstite + liquid and α-Fe-wollastonite$_{ss}$ + β-Fe-wollastonite$_{ss}$ + wüstite + liquid. In the 10^{-10} atm and 10^{-9} atm sections, the magnetite-wüstite inversion curve appears and

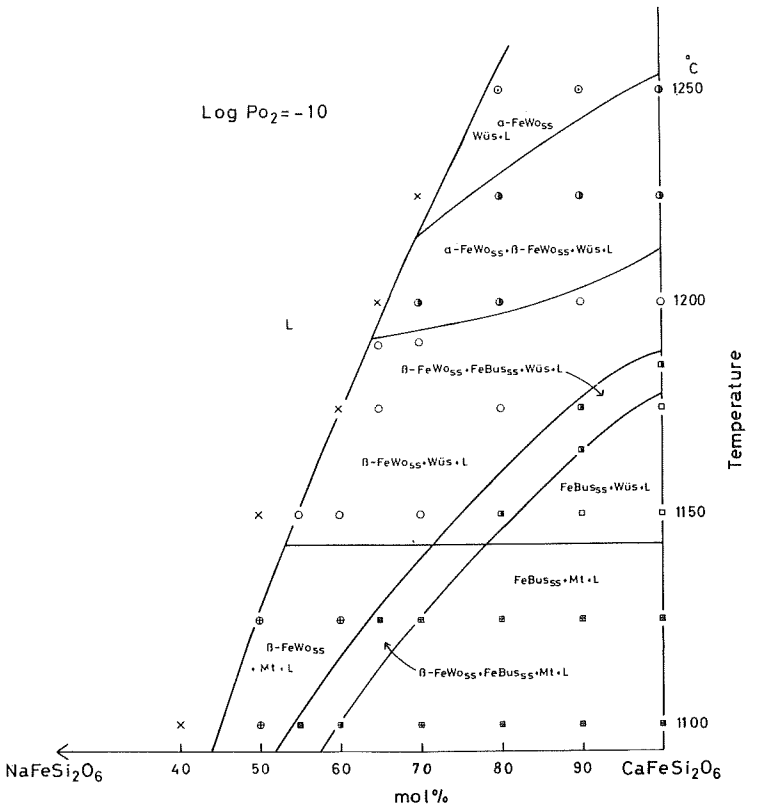

Fig. 7 Phase diagram of the system $NaFe^{3+}Si_2O_6$-$CaFe^{2+}Si_2O_6$ at 10^{-10} atm f_{O_2}. Abbrevations are given in Fig. 1.

crosses the divariant assemblage fields mentioned above, resulting in the presence of univariant assemblages: β-Fe-wollastonite$_{SS}$ + Fe-bustamite$_{SS}$ + wüstite + magnetite + liquid (10^{-10}) and α-Fe-wollastonite$_{SS}$ + β-Fe-wollastonite$_{SS}$ + wüstite + magnetite + liquid. Therefore, the univariant curve indicating these two assemblages has a positive slope in the T-f_{O_2} projection and must lie on the magnetite-wüstite inversion plane which is independent of the composition in the T-X-f_{O_2} space. These two univariant curves meet together at an invariant point where α-Fe-wollastonite$_{SS}$, β-Fe-wollastonite$_{SS}$, Fe-bustamite$_{SS}$ magnetite, and wüstite coexist with liquid.

When Fe^{3+} is not present at low f_{O_2}, say 10^{-11}, sodium can not enter into the crystalline phases in the form of $NaFe^{3+}Si_2O_6$, but all of this molecule is contained in the liquid. However, when magnetite is present, indicating the existence of Fe^{3+}, it is possible that some of the Fe^{3+}, in the form of $NaFe^{3+}Si_2O_6$, can be incorporated in the silicate phases and the remainder is contained in the liquid. The amount of Fe^{3+} in the silicate phases may increase

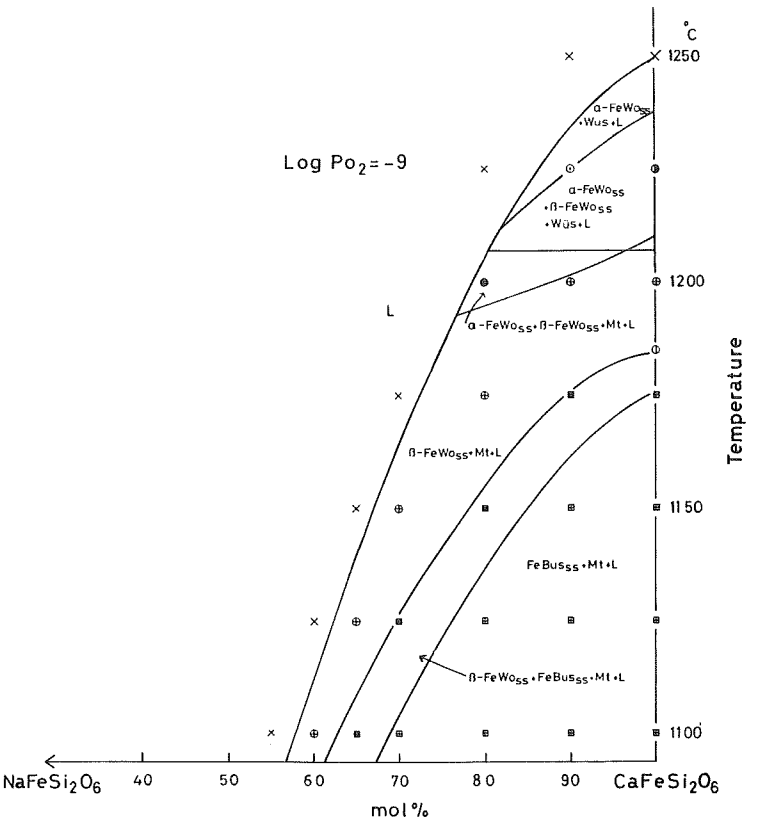

Fig. 8 Phase diagram of the system $NaFe^{3+}Si_2O_6$-$CaFe^{2+}Si_2O_6$ at 10^{-9} atm f_{O_2}. Abbrevations are given in fig. 1.

with decreasing amount of liquid and finally a complete series of solid solutions between $NaFe^{3+}Si_2O_6$ and $CaFe^{2+}Si_2O_6$ is formed at subsolidus temperatures as demonstrated by Ohashi (1976).

Application to natural pyroxene

The present experimental evidence supports the former conclusion of Yagi (1966) that at low f_{O_2} the pyroxene trend proceeds from diopsidic towards hedenbergitic and at high f_{O_2} from diopsidic through soda augite to aegirine. Recently Ewart et al. (1976) called attention to the fact that acmite-enrichment occurs only after extreme Fe-enrichment and not only f_{O_2} but activity of alumina in liquid plays an important role in determining the courses mentioned above. The presence of the acmite molecule in pyroxene also depends upon the concentration of calcium in the liquid. From their experimental studies Onuma and Yagi (1975) and Yoshikawa and Onuma (1975) suggested that at high f_{O_2}

when enough calcium and aluminum are present Fe^{3+} enters into pyroxene in the form of $CaFe^{3+}AlSiO_6$ and sodium forms nepheline, also that pyroxene proceeds towards acmite only when $Na > Fe^{3+} + Al$, as pointed out by Huckenholz (1973) in his study of natural pyroxene.

The above statement leads to the following conclusion: When f_{O_2} is higher than the magnetite-wüstite transition curve, pyroxene becomes acmitic in the case of $Na > Fe^{3+} + Al$, or fassaitic in the case of $Na < Fe^{3+} + Al$; when f_{O_2} is lower than the magnetite-wüstite curve, it becomes hedenbergitic in either case.

Acknowledgements

The authors' thanks are due to Mr. Haruo Ohashi of the National Institute for Research in Inorganic Materials for his help in the experimental technique, and Dr. N.C. Stevens of University of Queensland for his critical reading of the paper in manuscript. Part of the cost for the present study was defrayed by Grant for Scientific Research from the Ministry of Education of Japan, and a grant from the Mitsubishi Foundation.

References

Bowen, N.L., J.F. Schairer, and E. Posnjak, 1933. The system CaO-FeO-SiO_2. *Am. J. Sci.*, 26: 193-284.

Darken, L.S. and R.W. Gurry, 1945. The system iron-oxygen. I. The wüstite field and related equibria. *J. Am. Chem. Soc.*, 67: 1398-1412.

Ewart, A., A. Mateen and J.A. Ross, 1976. Review of mineralogy and chemistry of Tertiary central volcanic complexes in southeast Queensland and northeast New South Wales. *Volcanism in Australasia*, Ed. by R.W. Johnson, 21-39.

Huckenholz, I .G. 1973. The origin of fassaitic augite in the alkali basalt in suite of the Hocheifel area, Western Germany. *Contr. Min. Pet.*, 40: 315-326.

Lindsley, D.H., D.H. Speidel and R.H. Nafziger, 1968. P-T-f_0 relation for the system Fe-O-SiO_2. *Am. J. Sci.*, 266: 342-360.

Matsueda, H.,1973. Iron-wollastonite from the Sampo mine showing properties distinct from those of wollastonite. *Mineral. J.*, 7: 180-201.

Nolan, J., 1969. Physical properties of synthetic and natural pyroxenes in the system diopside-hedenbergite-acmite. *Mineral. Mag.*, 37: 216-229.

Ohashi, H., 1967. The system acmite-hedenbergite. M. Sc. Thesis Hokkaido Univ. (in Japanese).

Onuma, K. and K. Yagi, 1975. The join $CaMgSi_2O_6$-$CaAl_2SiO_6$-$CaFe^{3+}AlSiO_6$ in air and its bearing on fassaitic pyroxene. *J. Fac. Sci., Hokkaido Univ., Ser. 4*, 16: 343-356.

Peacor, D.R. and C.T. Prewitt, 1963. Comparison of the crystal structures of bustamite and wollastonite. *Am. Mineral.*, 48: 588-596.

Prewitt, C.T. and D.R. Peacor, 1964. Crystal chemistry of the pyroxenes and pyroxenoids. *Am. Mineral.*, 49: 1527-1542.

Rutstein, M.S., 1971. Re-examination of the wollastonite-hedenbergite ($CaSiO_3$-$CaFeSi_2O_6$)

equilibira. *Am. Mineral.*, 56: 2040-2052.

Rustein, M.S. and W.B. White, 1971. Vibrational spectra of high-calcium pyroxenes and pyroxenoids. *Am. Mineral.* 56: 877-887.

Yagi, K., 1966. The system acmite-diopside and its bearing on the stability relations of natural pyroxenes of the acmite-hedenbergite-diopside series *Am. Mineral.*, 51: 976-1000.

Yoshikawa, K. and K. Onuma, 1975. The join $NaFeSi_2O_6$-$CaAl_2SiO_6$ at 1 atmospheric and high pressure: Part I. Phase relations at 1 atm pressure in air. *J. Japan. Assoc. Min. Pet. Econ. Geol.*, 70: 335-346.

(Received on Oct. 21, 1976)

Appendix 1 Results of quenching experiments for the system $NaFe^{+3}Si_2O_6$ – $CaFe^{+2}Si_2O_6$ at 10^{-11} atm f_{O_2} and refractive indices of the pyroxenoids.

Composition (mol %) Ac	Hd	Temp. (°C)	Phases	Refractive indices (±0.003) α	γ	
0	100	1100	Fe-bus+wüs+gl	1.685	1.705	Fe-bus
		1125	Fe-bus+wüs+gl	1.680	1.700	Fe-bus
		1150	Fe-bus+wüs+gl	1.673	1.688	Fe-bus
		1175	Fe-bus+wüs+gl	1.654	1.669	Fe-bus
		1180	β-Fe-wo+Fe-bus+wüs+gl	1.651	1.664	Fe-bus
				1.628	1.642	β-Fe-wo
		1185	β-Fe-wo+Fe-bus+wüs+gl	1.650	1.663	Fe-bus
				1.628	1.641	β-Fe-wo
		1195	β-Fe-wo+wüs+gl	1.626	1.640	β-Fe-wo
		1200	β-Fe-wo+wüs+gl	1.627	1.641	β-Fe-wo
		1225	α-Fe-wo+β-Fe-wo+wüs+gl	1.625	1.638	β-Fe-wo
				1.609	1.652	α-Fe-wo
		1250	α-Fe-wo+β-Fe-wo+wüs+gl	1.624	1.638	β-Fe-wo
				1.609	1.653	α-Fe-wo
10	90	1100	Fe-bus+wüs+gl	1.675	1.691	Fe-bus
		1125	Fe-bus+wüs+gl	1.666	1.683	Fe-bus
		1150	Fe-bus+wüs+gl	1.655	1.669	Fe-bus
		1165	Fe-bus+wüs+gl	1.650	1.664	Fe-bus
		1175	β-Fe-wo+Fe-bus+wüs+gl	1.649	1.662	Fe-bus
				1.628	1.642	β-Fe-wo
		1185	β-Fe-wo+wüs+gl	1.626	1.640	β-Fe-wo
		1195	β-Fe-wo+wüs+gl	1.626	1.640	β-Fe-wo
		1200	β-Fe-wo+wüs+gl	1.626	1.640	β-Fe-wo
		1225	α-Fe-wo+β-Fe-wo+wüs+gl	1.624	1.638	β-Fe-wo
				1.609	1.653	α-Fe-wo
		1250	α-Fe-wo+wüs+gl	1.609	1.654	α-Fe-wo
20	80	1100	Fe-bus+wüs+gl	1.658	1.674	Fe-bus
		1125	Fe-bus+wüs+gl	1.655	1.669	Fe-bus
		1150	Fe-bus+wüs+gl	1.649	1.663	Fe-bus
		1165	β-Fe-wo+Fe-bus+wüs+gl	1.647	1.662	Fe-bus
				1.628	1.642	β-Fe-wo
		1175	β-Fe-wo+wüs+gl	1.626	1.640	β-Fe-wo
		1195	β-Fe-wo+wüs+gl	1.625	1.639	β-Fe-wo
		1200	α-Fe-wo+β-Fe-wo+wüs+gl	1.622	1.636	β-Fe-wo
				1.610	1.653	α-Fe-wo
		1225	α-Fe-wo+β-Fe-wo+wüs+gl	1.623	1.636	β-Fe-wo
				1.609	1.653	α-Fe-wo
		1250	α-Fe-wo+wüs+gl	1.609	1.653	α-Fe-wo

Appendix 1 (continued)

Composition (mol %) Ac	Hd	Temp. (°C)	Phases	Refractive indices (±0.003) α	γ	
30	70	1100	Fe-bus+wüs+gl	1.655	1.668	Fe-bus
		1125	Fe-bus+wüs+gl	1.652	1.665	Fe-bus
		1150	β-Fe-wo+wüs+gl	1.626	1.639	β-Fe-wo
		1175	β-Fe-wo+wüs+gl	1.622	1.634	β-Fe-wo
		1195	α-Fe-wo+β-Fe-wo+wüs+gl	1.622	1.636	β-Fe-wo
				1.609	1.654	α-Fe-wo
		1225	α-Fe-wo+wüs+gl	1.609	1.653	α-Fe-wo
		1250	α-Fe-wo+wüs+gl	1.609	1.652	α-Fe-wo
35	65	1125	β-Fe-wo+Fe-bus+wüs+gl	1.648	1.662	Fe-bus
				1.628	1.642	β-Fe-wo
		1185	β-Fe-wo+wüs+gl	1.625	1.639	β-Fe-wo
		1200	α-Fe-wo+β-Fe-wo+wüs+gl	1.623	1.636	β-Fe-wo
				1.609	1.653	α-Fe-wo
		1225	α-Fe-wo+wüs+gl	1.610	1.653	α-Fe-wo
		1250	gl			
40	60	1100	Fe-bus+wüs+gl	1.652	1.666	Fe-bus
		1125	β+Fe-wo+wüs+gl	1.626	1.640	β-Fe-wo
		1150	β-Fe-wo+wüs+gl	1.624	1.638	β-Fe-wo
		1175	β-Fe-wo+wüs+gl	1.624	1.637	β-Fe-wo
		1185	β-Fe-wo+wüs+gl	1.624	1.638	β-Fe-wo
		1200	α-Fe-wo+β-Fe-wo+wüs+gl	1.621	1.635	β-Fe-wo
				1.610	1.653	α-Fe-wo
		1225	gl			
45	55	1100	β-Fe-wo+Fe-bus+wüs+gl	1.649	1.663	Fe-bus
				1.627	1.641	β-Fe-wo
		1175	β-Fe-wo+wüs+gl	1.624	1.636	β-Fe-wo
		1200	gl			
50	50	1100	β-Fe-wo+wüs+gl	1.627	1.640	β-Fe-wo
		1125	β-Fe-wo+wüs+gl	1.625	1.638	β-Fe-wo
		1150	β-Fe-wo+wüs+gl	1.623	1.634	β-Fe-wo
		1175	gl			
60	40	1100	β-Fe-wo+wüs+gl	1.623	1.636	β-Fe-wo
		1125	gl			
70	30	1100	gl			

Abbrevations are given in Fig. 1.

Appendix 2 Results of quenching experiments for the system $NaFe^{+3}Si_2O_6$ – $CaFe^{+2}Si_2O_6$ at 10^{-10} atm f_{O_2} and refractive indices of the pyroxenoids.

Composition (mol %) Ac	Hd	Temp. (°C)	Phases	Refractive indices (±0.003) α	γ	
0	100	1100	Fe-bus+mt+gl	1.683	1.700	Fe-bus
		1125	Fe-bus+mt+gl	1.674	1.691	Fe-bus
		1150	Fe-bus+wüs+gl	1.667	1.681	Fe-bus
		1165	Fe-bus+wüs+gl	1.653	1.667	Fe-bus
		1175	Fe-bus-wüs+gl	1.650	1.664	Fe-bus
		1185	β-Fe-wo+Fe-bus+wüs+gl	1.648	1.663	Fe-bus
				1.629	1.642	β-Fe-wo
		1190	β-Fe-wo+wüs+gl	1.628	1.641	β-Fe-wo
		1200	β-Fe-wo+wüs+gl	1.628	1.641	β-Fe-wo
		1225	α-Fe-wo+β-Fe-wo+wüs+gl	1.627	1.640	β-Fe-wo
				1.609	1.653	α-Fe-wo
		1250	α-Fe-wo+β-Fe-wo+wüs+gl	1.623	1.636	β-Fe-wo
				1.609	1.652	α-Fe-wo
10	90	1100	Fe-bus+mt+gl	1.670	1.683	Fe-bus
		1125	Fe-bus+mt+gl	1.663	1.678	Fe-bus
		1150	Fe-bus+wüs+gl	1.655	1.669	Fe-bus
		1165	β-Fe-wo+Fe-bus+wüs+gl	1.649	1.663	Fe-bus
				1.628	1.641	β-Fe-wo
		1175	β-Fe-wo+Fe-bus+wüs+gl	1.649	1.662	Fe-bus
				1.628	1.641	β-Fe-wo
		1185	β-Fe-wo+wüs+gl	1.626	1.640	β-Fe-wo
		1200	β-Fe-wo+wüs+gl	1.626	1.639	β-Fe-wo
		1225	α-Fe-wo+β-Fe-wo+wüs+gl	1.625	1.638	β-Fe-wo
				1.609	1.653	α-Fe-wo
		1250	α-Fe-wo+wüs+gl	1.609	1.652	α-Fe-wo
20	80	1100	Fe-bus+mt+gl	1.655	1.669	Fe-bus
		1125	Fe-bus+mt+gl	1.651	1.665	Fe-bus
		1150	β-Fe-wo+Fe-bus+wüs+gl	1.648	1.662	Fe-bus
				1.629	1.642	β-Fe-wo
		1200	α-Fe-wo+β -Fe-wo+wüs+gl	1.621	1.638	β-Fe-wo
				1.609	1.654	α-Fe-wo
		1225	α-Fe-wo+β-Fe-wo+wüs+gl	1.623	1.636	β-Fe-wo
				1.609	1.653	α-Fe-wo
		1250	α-Fe-wo+wüs+gl	1.609	1.653	α-Fe-wo
30	70	1100	Fe-bus+mt+gl	1.654	1.658	Fe-bus
		1125	Fe-bus+mt+gl	1.650	1.664	Fe-bus
		1150	β-Fe-wo+wüs+gl	1.626	1.640	β-Fe-wo
		1190	β-Fe-wo+wüs+gl	1.622	1.636	β-Fe-wo

Appendix 2 (continued)

Composition (mol %) Ac	Hd	Temp. (°C)	Phases	Refractive indices (±0.003) α	γ	
		1200	α-Fe-wo+β-Fe-wo+wüs+gl +gl	1.620	1.634	β-Fe-wo
				1.609	1.653	α-Fe-wo
		1225	gl			
35	65	1125	β-Fe-wo+Fe-bus+mt+gl	1.648	1.662	Fe-bus
				1.628	1.642	β-Fe-wo
		1175	β-Fe-wo+wüs+gl	1.624	1.637	β-Fe-wo
		1190	β-Fe-wo+wüs+gl	1.622	1.636	β-Fe-wo
		1200	gl			
40	60	1100	Fe-bus+mt+gl	1.650	1.664	Fe-bus
		1125	β-Fe-wo+mt+gl	1.626	1.640	β-Fe-wo
		1150	β-Fe-wo+wüs+gl	1.623	1.636	β-Fe-wo
		1175	gl			
45	55	1100	β-Fe-wo+Fe-bus+mt+gl	1.648	1.662	Fe-bus
				1.627	1.642	β-Fe-wo
		1150	β-Fe-wo+wüs+gl	1.622	1.635	β-Fe-wo
50	50	1100	β-Fe-wo+mt+gl	1.623	1.635	β-Fe-wo
		1125	β-Fe-wo+mt+gl	1.622	1.635	β-Fe-wo
		1150	gl			
60	40	1100	gl			

Abbrevations are given in Fig. 1.

Appendix 3 Results of quenching experiments for the system $NaFe^{+3}Si_2O_6$ – $CaFe^{+2}Si_2O_6$ at 10^{-9} atm f_{O_2} and refractive indices of the pyroxenoids.

Composition (mol %) Ac	Hd	Temp. (°C)	Phases	Refractive indices (±0.003) α	γ	
0	100	1100	Fe-bus+mt+gl			
		1125	Fe-bus+mt-gl	1.671	1.687	Fe-bus
		1150	Fe-bus+mt-gl	1.666	1.680	Fe-bus
		1175	Fe-bus+mt-gl	1.650	1.665	Fe-bus
		1185	β-Fe-wo+mt+gl	1.626	1.640	β-Fe-wo
		1200	β-Fe-wo+mt+gl	1.624	1.638	β-Fe-wo
		1225	α-Fe-wo+β-Fe-wo+wüs+gl	1.623	1.636	β-Fe-wo
				1.608	1.653	α-Fe-wo
10	90	1100	Fe-bus+mt+gl	1.666	1.680	Fe-bus
		1125	Fe-bus+mt+gl	1.659	1.672	Fe-bus
		1150	Fe+bus+mit+gl	1.651	1.666	Fe-bus
		1175	β-Fe-wo+Fe-bus+mt+gl	1.647	1.662	Fe-bus
				1.627	1.641	β-Fe-wo
		1200	β-Fe-wo+mt+gl	1.625	1.638	β-Fe-wo
		1225	α-Fe-wo+wüs+gl	1.609	1.653	α-Fe-wo
		1250	gl			
20	80	1100	Fe-bus+mt+gl	1.655	1.668	Fe-bus
		1125	Fe-bus+mt+gl	1.653	1.666	Fe-bus
		1150	β-Fe-wo+Fe-bus+mt+gl	1.647	1.661	Fe-bus
				1.627	1.640	β-Fe-wo
		1175	β-Fe-wo+mt+gl	1.627	1.640	β-Fe-wo
		1200	α-Fe-wo+β-Fe-wo+mt+gl	1.625	1.638	β-Fe-wo
				1.609	1.651	α-Fe-wo
		1225	gl			
30	70	1100	Fe-bus+mt+gl	1.650	1.664	Fe-bus
		1125	β-Fe-wo+Fe-bus+mt+gl	1.648	1.662	Fe-bus
				1.627	1.641	β-Fe-wo
		1150	β-Fe-wo+mt+gl	1.628	1.641	β-Fe-wo
		1175	gl			
35	65	1100	β-Fe-wo+Fe-bus+mt+gl	1.647	1.664	Fe-bus
				1.628	1.642	β-Fe-wo
		1125	β-Fe-wo+mt+gl	1.625	1.638	β-Fe-wo
		1150	gl			
40	60	1100	β-Fe-wo+mt+gl	1.623	1.636	β-Fe-wo
		1125	gl			
45	55	1100	gl			

Abbrevations are given in Fig. 1.